INS-NUMA-50

Characteristics of Sextupole Magnets for TARN

A. Noda, S. Kadota and M. Takanaka

April, 1983

STUDY GROUP OF NUMATRON AND HIGH-ENERGY HEAVY-ION PHYSICS
INSTITUTE FOR NUCLEAR STUDY
UNIVERSITY OF TOKYO
Midori-Cho 3-2-1, Tanashi-Shi,
Tokyo 188, Japan

INS-NUMA-50
April, 1983

Characteristics of Sextupole Magnets for TARN

A. Noda, S. Kadota and M. Takanaka

Institute for Nuclear Study, University of Tokyo

Abstract

A correction system of chromaticities with use of sextupole magnets has been installed in TARN. Twelve magnets are devided into two families, SF and SD, which locate places with different twiss parameters to adjust chromaticities in horizontal and vertical directions indepent on each other.

The sextupole magnet can excite the integrated sextupole strength ($\int B''ds$) of 66 kG/m for the excitation current of 400 A to attain enough chromaticity size for N^{5+} with kinetic energy of 8.55 MeV/u.

With the sextupole system, working line nearly parallel to the difference resonance $\nu_x - \nu_z = 0$ has been realized. The chromaticities for this working line calculated by an analytical method with use of sextupole strength are -2.48 and -2.27 for horizontal and vertical directions, respectively, which are quite in good agreement with experimentary measured ones of -2.47 and -2.23.

1. Introduction

At TARN, where relatively low energy (8.5 MeV/u) ion beam is to be accumulated, the transverse resistive wall instability would become sereve problem when accumulated beam increases. In order to surmount this instability by Landau damping, a chromaticity correction system with sextupole magnets has been designed[1].

The contribution of sextupole magnets to the chromaticities is given by

$$\left.\begin{aligned} \frac{d\nu_x}{d\delta} &= \frac{1}{4\pi}\int \frac{B''}{B\rho}\,\eta\beta_x ds \\ \frac{d\nu_y}{d\delta} &= -\frac{1}{4\pi}\int \frac{B''}{B\rho}\,\eta\beta_y ds \quad , \end{aligned} \qquad \left(\delta = \frac{\Delta P}{P}\right) \right\} \tag{1}$$

where ν_x and ν_y are number of betatron oscillations per turn in horizontal and vertical directions, respectively, β_x and β_y are horizontal and vertical beta-function, respectively and η denotes dispersion function.

From these equations, it is known that so as to control both horizontal and vertical chromaticities, two families of sextupole magnets which locate at the positions where β_x, β_y and η have different values from each other are needed. When two families (SF and SD) as shown in Fig. 1 are used, the maximum sextupole strength of 300 kG/m^2 is needed for $^{14}N^{5+}$ beam. In real fabrication, this value is set to be 350 kG/m^2 so as to leave flexibility of adjustment. From the point of view of installation into TARN, the core length and bore radius of the sextupole magnet are determined to be 0.1 m and 0.135 m, respec tively, which enabled the installation of these magnets with vacuum chambers already existing.

In the present paper, the design of the sextupole magnet is described in section 2. In section 3, the procedure and the result of the field measurement is given. Finally the effect of the sextupole magnets to the working line experimentally studied are given in section 4.

2. Design of the Sextupole Magnet

If we consider the ideal case where six line currents with infinite length are flowing in $\pm$ s direction as shown in Fig. 2, where s direction is perpendicular to the paper plane. This configuration is invariant for rotation of $\frac{2\pi}{3}$ around s axis, so the complex potential $W(\xi)$ can be written as[2)]

$$W(\xi) = \sum_{n=0}^{\infty} a_{3n}\xi^{3n} \quad , \tag{2}$$

where $\xi = x + iy$. The term of $n = 1$ represents the sextupole field of our concern. The magnetic scalar potential ϕ_m is given by the imaginary part of $W(\xi)$ and can be written as

$$\phi_m(\xi) = \sum_{n=0}^{\infty} a_{3n} r^{3n} \sin 3n\theta \quad , \tag{3}$$

where r and θ are polar coordinate of ξ. If the higher terms are absent, the curve which satisfies the relation;

$$a_3 r^3 \sin 3\theta = k \text{ (const)} \tag{4}$$

represents the equi-potential line of the magnetic potential. The equation (4) represents a cubic equation

$$3x^2y - y^3 = \frac{k}{a_3} \text{ (const)}. \tag{5}$$

If we assume the infinitely large permeability of iron, the pole surface of the magnet should coincide with this equi-potential surface. The equation (5) can be written as

$$3x^2y - y^3 = - r_o^{\ 3} \tag{6}$$

with use of the bore radius, r_o, of the magnet. From the Ampere's law, the following relation can be derived if the infinitely large permeability of iron is assumed,

$$NI = \frac{1}{6\mu_o} B'' r_o^{\ 3} \quad , \tag{7}$$

where μ_o is the permeability in the air, B'' represents sextupole strength $(\frac{d^2 By}{dx^2})$ and NI is ampere-turn per pole.

From the point of view of attaining the required aperture for TARN, which is much larger in horizontal direction compared with the vertical direction, it might be an idea to use a deformed pole shape which is wider in horizontal direction. However, as the case of quadrupole magnet[3], we have decided to make a symmetric pole with 6-fold symmetry to realize the good field property.[4] As is known from Fig. 3, if the pole shape has complete six-fold symmetry the magnetic scalar potential $\phi_m(\xi)$ only changes sign when rotation of $\frac{\pi}{3}$ around s axis is applied. Then the following relation exists

$$\phi_m(\theta \pm \frac{\pi}{3}) = -\phi_m(\theta) \quad . \tag{8}$$

Using equation (3), this relation leads to

$$a_{3n} r^{3n} \sin\{3n(\theta \pm \frac{\pi}{3})\} = -a_{3n} r^{3n} \sin 3n\theta \quad . \tag{9}$$

So as to assure the relation (9) for arbitrary value of θ, the following relation should hold

$$a_{3n} = 0 \quad \text{for} \quad n = 2\ell \quad (\ell = 0,\ 1,\ 2, \cdots) \ . \tag{10}$$

Thus the magnetic scalar potential can be expressed as

$$\phi_m = \sum_{\ell=0}^{\infty} a_{3(2\ell+1)} \cdot r^{3(2\ell+1)} \sin 3(2\ell+1)\theta \quad , \tag{11}$$

which leads to the field component as follows

$$By = -\frac{\partial\phi_m}{\partial y}$$

$$= -\frac{\partial}{\partial y}\,[a_3 r^3 \sin 3\theta + a_9 r^9 \sin 9\theta + \cdots\ ]$$

$$= -\ [3a_3(x^2 - y^2) + a_9(9x^8 - 252x^6 y2 + 630x^4 y^4 - 252x^2 y^6 + 9y^8)\cdots\ ] \quad (12)$$

which becomes in the median plane as

$$By = -[\ 3a_3x^2 + 9a_9x^8 + \cdots\ ]\quad , \qquad (13)$$

thus the higher multipoles such as octapole, decapole and dodecapole etc. except the one of x^8 are absent if the fabrication error does not exist.

As is described in section 1, the core length and bore radius of the sextupole magnet are determined at 0.1 m and 0.135 m, respectively considering the available space for installation of the magnet. From Eq. (7), the necessary ampere-turn to attain 350 kG/m^2 for the present magnet is calculated at 11420 AT per pole. In the calculation, however, the effect of finite permeability of the iron and the fringing field effect are neglected and in the present case the latter fringing field effect is anticipated rather large because the bore radius is large compared with the core length. Taking this fact into account, the ampere-turn is determined at 16400 AT per pole in real fabribation. The pole shape is decided to be made by the ideal shape

$$3x^2y - y^3 = \pm\ r_o^{\ 3} \qquad (14)$$

given in the above discussion and the pole width is set to be 104 mm to make coil space of finite size. Field calculation was executed by the computer code TRIM with the MESH given in Fig. 4(a) and the calculated flux line for the sextupole strength of 300 kG/m^2 is shown in Fig. 4 (b).

In Fig. 5, dependence of the calculated field (By) and the sextupole strength ($B'' = \frac{d^2By}{dx^2}$) on the radial position is given. From the figure, it is known that the sextupole strength is flat in the region ± 70 mm, where multi-turn injected and RF stacked beams exist as shown in Fig. 6.

Drawing of real fabricated magnet is given in Fig. 7 and the specifications of the magnet is listed up in Table 1.

It should be noted that in real magnet, the fringing field effect appears different from the two dimensional calculation by the computer code TRIM. Therefore it is necessary to study how the sextupole magnet affect the beam motion. From the equation of motion:

$$Am_n\gamma\frac{d^2\vec{x}}{dt^2} = qe[\vec{v}\times\vec{B}] \quad , \qquad (15)$$

where A, q and m_n are mass number, charge state of the ion and atomic mass unit, respectively, the following equations can be derived,

$$\left.\begin{aligned} \frac{d^2x}{ds^2} &= -\frac{B_y}{B\rho} \\ \frac{d^2y}{ds^2} &= \frac{B_x}{B\rho} \quad , \end{aligned}\right\} \qquad (16)$$

where $B\rho$ is the magnetic rigidity of the ion beam, which can be written as $(B\rho)_o\ (1+\frac{\Delta P}{P})$ with use of magnetic rigidity $(B\rho)_o$ of the beam with the central momentum and fractional momentum deviation $\frac{\Delta P}{P}$.

In the present case, the core length of the sextupole magnet is rather short (0.1 m) compared with the wave length of betatron oscillation ($\sim$ 14 m), the following relation can be obtained from equations (16),

$$\left.\begin{aligned} \left.\frac{dx}{ds}\right|_2 - \left.\frac{dx}{ds}\right|_1 &= -\frac{By\cdot\ell}{(B\rho)_o(1+\frac{\Delta P}{P})} \\ \left.\frac{dy}{ds}\right|_2 - \left.\frac{dy}{ds}\right|_1 &= \frac{B_x\cdot\ell}{(B\rho)_o(1+\frac{\Delta P}{P})} \quad , \end{aligned}\right\} \qquad (17)$$

where suffix 1 and 2 denote the entrance and exit points of the magnet, and ℓ represents its ellective length, respectively. From magnetic scalar potential (11) and the relation

$$- 6a_3 = B'' \quad , \tag{18}$$

the equations (17) can be rewritten as

$$\left.\begin{aligned} \frac{dx}{ds}\Big|_2 - \frac{dx}{ds}\Big|_1 &= - \frac{B''\cdot\ell}{2(B\rho)_0(1+\frac{\Delta P}{P})} (x^2 - y^2) \\ \frac{dy}{ds}\Big|_2 - \frac{dy}{ds}\Big|_1 &= \frac{B''\cdot\ell}{(B\rho)_0(1+\frac{\Delta P}{P})} xy \quad . \end{aligned}\right\} \tag{19}$$

From the above equations (19), the value of $B''\cdot \ell$ which denotes $\int B''ds$, is important one as the measure for the effect of sextupole field. So as to study the structure of $\int B''ds$, three dimensional calculation or field measurement is needed. We have decided to execute a field measurement.

The flat region of the effective length is expected to be enlarged by the end-cut similar to the case of the quadrupole magnet.[3)5)] In the present case, three different end-cut shapings given in Fig. 8 are made for the first constructed sextupole magnet and the field measurement with translation coils[3)6)] are applied for these end-cut shapings. Pole shape 2 is calculated from the end-cut shape of the quadrupole magnet for TARN[3)] by scaling of bore radii. The obtained results are given in Fig. 9 and from the figure it is known that end-cut shape 2 is the best among these shapes. So the end-cut shape is finally determined to be shape 2 and the other eleven magnets are made by this shape from the first.

3. Field Measurement and Characteristics of the Sextupole Magnet

The field structure of the sextupole magnets has been measured by two independent methods so as to cross check the reliability of each system. One of which utilizes a temperature-controled Hall-probe calibrated by an NMR in a uniform field and the other uses the twin translation coils.

3.1. Measurement of Absolute Sextupole Strength and its Effective Length by a Hall-probe

In order to evaluate the absolute strength of the sextupole magnet, field mapping has been executed with use of the measurement system developed for the dipole magnets of TARN,[7] which utilize a temperature controled Hall-probe. Its calibration has been done previously in a uniform field with use of proton resonance. The position of the probe can be controled in a horizontal plane by two pulse motors attached to ball-screws. The measurement system applied to the sextupole magnet is shown in Fig. 10. The system is operated fully automatically by a mini-computer HP-1000 system and the measured data have been monitored by real time with the computer system. In Fig. 11, an example of the mapped field strength displayed on a graphic display terminal is shown. These mapped values are numerically integrated along the line of constant x (x denote the distance from the magnet axis in the median plane), which gives $\int Byds$ for each value of x as shown in Fig. 12. Fitting $\int Byds$ by a polynomial as follows

$$\int Byds = \sum_n a_n x^n = a_o + a_1 x + a_2 x^2 + \cdots \quad , \tag{20}$$

the integrated sextupole strength, $\int By''ds$, can be given by $2a_2$ and the results are shown in Fig. 13 (a). Similar polynomial fitting is executed for the mapped data, By, at the position of $s=0$ as

$$By(x,0) = \sum_n b_n x^n = b_o + b_1 x + b_2 x^2 + \cdots \quad , \tag{21}$$

which gives the value $By''(x,0)$ by $2b_2$ and the results are shown in Fig. 13 (b). Combining these two results, the effective length of the magnet can be obtained as shown in Fig. 13 (c). Due to the fact that the bore radius is larger compared with the core length, the effective length is rather large (196 mm) compared with the iron length (100 mm).

The excitation characteristics of the sextupole magnet has been studied fixing the Hall-probe at $x = 100$ mm (Fig. 14) and the effect of saturation of iron core is found very small even at the excitation current of 400 A.

3.2. Measurement of Field Structure by Twin Translation Coils

For the purpose of studying the field structure, twin translation coils system developed for the quadrupole magnet of TARN[3)] is preferable, because the system directly measures the sextupole strength and higher components. The measuring system applied to the sextupole magnet is shown in Fig. 15. As is anticipated from the fact that the core length is shorter compared with its bore radius, the flat region of the field strength in the direction of magnet axis does not exist (Fig. 11). On the other hand, in the present case where the thin lens approximation is appropriate as is discussed in the previous section, the important value which affects beam motion is only the integrated sextupole strength, $\int B_y''ds$. So, long twin translation coils with the length of 774 mm are used. This length is long enough to cover the effective field length of 196 mm discussed in the previous section. The difference of induced voltages at twin coils are directly measured by hard wire connection as shown in Fig. 16. The measurement is performed with two states ("Up" and "Down" states shown in the figure) to cancel out the asymmetry of the geometries of these coils. Let's denote the induced signals ΔV_{up} and ΔV_{down} obtained at "Up" and "Down" states, respectively, then the sum of these values, ΔV, gives the sextupole and higher components integrated along the magnet axis as follows,

$$\Delta V(x) = CN(d_1 + d_2)\left[\int_{-\infty}^{\infty} \frac{\partial B_y}{\partial x}\Big|_{x+\frac{\Delta x}{2}} \cdot ds - \int_{-\infty}^{\infty} \frac{\partial B_y}{\partial x}\Big|_{x-\frac{\Delta x}{2}} \cdot ds\right]\Delta x \quad , \qquad (22)$$

where d_1 and d_2 are widths of the twin coils, N is the turn number of each coil (in the present case N = 701) and C is the calibration constant which depends on the characteristics of the electronics system to measure the induced voltage.[3] Taking the ratio of $\Delta V(x)$ and $\Delta V(0)$, these constants can be cancelled out and the following relation is obtained

$$\frac{\Delta V(x)}{\Delta V(0)} = \frac{\left[\int_{-\infty}^{\infty} \frac{\partial By}{\partial x}\Big|_{x+\frac{\Delta x}{2}} ds - \int_{-\infty}^{\infty} \frac{\partial By}{\partial x}\Big|_{x-\frac{\Delta x}{2}} ds\right]}{\left[\int_{-\infty}^{\infty} \frac{\partial By}{\partial x}\Big|_{\frac{\Delta x}{2}} ds - \int_{-\infty}^{\infty} \frac{\partial By}{\partial x}\Big|_{-\frac{\Delta x}{2}} \cdot ds\right]} \quad . \tag{23}$$

In Fig. 17, the measured data for three excitation currents (200 A, 300 A and 400 A) are shown and it is known from the figure that difference of the field structures among different excitation currents is quite small, which indicates the saturation effect of iron is so small. Field structures for median plane and $\pm$ 15 mm apart from it are shown in Fig. 18. In the median plane, flat region of $\int B''ds$ is the narrowest. This is considered due to the fact that the fringing field effect is the largest in the median plane. It is found from the figure that the variation of the integrated sextupole strength is below $\pm$ 0.8 % in the region for beam accumulation of $\pm$ 70 mm even in the median plane.

3.3. Cross Check between Two Measurements

The radial distribution of the integrated sextupole strength is measured by two method, one by integrating the mapped data with a Hall-probe and the other by twin translation coils. In Fig. 19, the results by these methods are compared. Although some deviations are observed at the both ends around $\pm$ 100 mm, the consistency in the region of our concern ($x = -70$ mm $\sim +70$ mm) is quite good.

The excitation characteristic of the magnet is also studied by these two methods (Fig. 20) and the agreement between two methods is quite good.

3.4. Multi-pole Components obtained by Polynomial Fitting

From the measured data with use of twin translation coils, $\frac{\Delta(\int B''ds)}{(\int B''ds)_0}$ is known for various radial position x (Figs. 17 and 18).

Fitting these data by a polynomial of x, the higher multi-pole components from sextupole can be obtained. So as to make the coefficients of the polynomial to be dimensionless, the expansion is done for $(\frac{x}{r_o})$ as follows

$$\int_{-\infty}^{\infty} B''(x,s)ds = \int_{-\infty}^{\infty} B''(0,s)ds \left[a_1 + a_2 \left(\frac{x}{r_o}\right) + a_3 \left(\frac{x}{r_o}\right)^2 + \cdots + a_n \left(\frac{x}{r_o}\right)^{n-1} + \cdots \right], \tag{24}$$

where r_o is the bore radius of the magnet. The resultant coefficients of the polynomial fitting is listed up in Table 2. The features of each coefficient among magnets are given in Table 3, which shows a_1 and a_7 are larger compared with other coefficients ($a_2 \sim a_6$). This fact shows that the six-fold symmetry imposed on the magnet has really suppressed the appearance of higher multipoles corresponding $a_2 \sim a_6$ as discussed in section 2. As is known from table 3, octapole (a_2), decapole (a_3), dodecapoles (a_4) and so on up to a_6 are not only small in their absolute value, but also change their signs from magnet to magnet, so these appear not from the design, but from the fabrication errors, which proved the validty of our design principle.

3.5. Deviation of Sextupole Strength among Magnets and their Alignment

In table 4, the sextupole strengths for the same excitation current of 400 A are listed up for all twelve sextupole magnets and the deviation of the strength of each magnet from the average are shown in Fig. 21. The deviation is $-0.51 \sim +0.62$ % for all these magnets, but asigning the magnets with similar characteristics to the same family as shown in the figure, the deviation in the same family can be reduced to $\pm$ 0.3 %.

These magnets have been installed into the TARN at the position shown in Fig. 1. The accuracy of the alignment is listed up in table 5 with the notation given in Fig. 22.

4. Chromaticity Correction realized by the Sextupole-Magnet System

At TARN, beam experiments of RF stacking have largely proceeded in these three years.[8] In the process, various working lines are tested

In Fig. 23, typical examples of sextupoles on and off are shown.

Natural chromaticities at line A for proton with the kinetic energy of 7 MeV are measured with use of the RF knock-out method[9] to be -1.93 and -0.63 for horizontal and vertical directions, respectively, while the calculated ones by SYNCH code[10] are -4.54 and -1.26, respectively. The effect of sextupole magnet system to the ν-values has been studied. In Fig. 24, the ν-values measured at various sweep frequencies of RF stacking (Δf) are plotted for the cases of the sextupole magnet system on ($\int B''ds$ = 2.6 kG/m for SD family and $\int B''ds$ = -2.6 kG/m for SF family) and off under other conditions the same (dipole field = 2.87 kG, GF = 6.37 kG/m, GD = 10.99 kG/m). From solid (sextupole off) and dashed (sextupole on) lines of the figure, working lines A and B in Fig. 23 are derived.

From the measured values of natural chromaticities ($\xi_{ox} = -1.93$, $\xi_{oy} = -0.63$) for line A and the excited strengths of sextupole magnet families ($\int B''ds$ = 2.6 kG/m for SD and $\int B''ds$ = -2.6 kG/m for SF), chromaticities for line B are calculated at -2.48 and -2.27 for ξ_x and ξ_y, respectively from the formulae[1)]

$$\left.\begin{aligned} \xi_x &= \xi_{ox} + \sum_{i=1}^{2} a_i S_i \\ \xi_y &= \xi_{oy} + \sum_{i=1}^{2} b_i S_i \quad , \end{aligned}\right\} \qquad (25)$$

where suffix i denotes the two families of sextupole magnets, S_i presents the sextupole strength of i-th family ($S_i = \frac{(\int B''ds)_i}{B\rho}$), and

$$\begin{bmatrix} a_i \\ b_i \end{bmatrix} = \frac{N_i n_i}{4\pi} \begin{bmatrix} \beta_{xi} \\ -\beta_{yi} \end{bmatrix} \qquad (26)$$

(N_i : number of sextupole magnets of i-th family).

Corresponding values of chromaticites for line B are also calculated with the tracking routine of the computer code SYNCH to be -5.09 and -2.90 for ξ_x and ξ_y, respectively.

Measured values of ξ_x and ξ_y for line B are -2.47 and -2.23, respectively which are quite in good agreement with the calculation by Eqs. (25) and (26). Some discrepancy of SYNCH calculation seems due to the fact that at TARN, the radius of curvature (1.333 m) is the same order as the dispersion function (0.97 ∿ 1.65 m) and the bending magnets are fan-shaped.[11)]

Acknowledgements

The authors would like to present their sincere thanks to Profs. K. Sugimoto and Y. Hirao for their continuous encouragements during the work. They are also grateful to Prof. T. Katayama for the excellent leadership for TARN beam experiments and fruitful discussion. Their thanks are also due to Prof. A. Mizobuch for various important suggestions in the process of construction of sextupole magnets.

This work has been performed under the collaboration of all the members of accelerator group for NUMATRON project. The authors would like to express their hartful thanks to all the members of this group.

They are also indebted to Messrs. Honma, H. Furuya and other members of the machine shop at INS for strong support in the process of alignment of the magnets.

One of the authors (A. N.) would like to present his sincere thanks to Dr. A. Garren from Lawrence Berkeley Laboratory for collaboration in the design process of the system.

Computer calculation with SYNCH was performed with M180 II AD at INS and field calculation with the computer code TRIM was done by HITAC 8800 at KEK.

References

1) A. Garren and A. Noda, "A Sextupole Magnet Correction System for TARN", INS-NUMA-14 (1979).

2) H. Ikegami, Butsuri. 34 (1979) 778 (in Japanese).

3) A. Noda, M. Mutou, T. Hattori, Y. Hirao, T. Hori, T. Katayama and H. Sasaki, "Quadrupole Magnet for TARN", INS-NUMA-23 (1980).

4) G. Parzen, "Magnetic Fields for Transporting Charged Beams", Brookhaven National Laboratory, preprint, ISA-76-13.

5) M. Kumada, H. Someya, I. Sakai and H. Sasaki, "Wide Aperture Q Magnet with End Cut Shaping", Proc. of 2nd Symp. on Acc. Sci. & Tech. (1978) 75.

6) M. Kumada, I. Sakai, H. Someya and H. Sasaki, "Flux Meter for Field Gradient with Pendulum", Proc. of 2nd Symp. on Acc. Sce. & Tech. (1978) 73.

7) T. Hori, A. Noda, T. Hattori, T. Fujino, M. Yoshizawa, T. Nakanishi, T. Katayama, Y. Hirao and H. Sasaki, "Field Measurement of Dipole Magnets for TARN", INS-NUMA-24 (1980).

8) T. Katayama et al., "BEAM STACKING EXPERIMENTS AT TARN", Proc. of 4th Symp. on Acc. Sci. & Tech. (1982) 23.

9) A. Noda et al., "Measurement of ν-values for TARN by the RF Knock-out Method", INS-NUMA-27 (1980).

10) A. A. Garren and J. W. Eusebio, Lawrence Radiation Laboratory Report, UCID-10154 (1965).

11) J. Jäger and D. Möhl, "COMPARISON OF METHODS TO EVALUATE THE CHROMATICITY IN LEAR", CERN PS/DL/LEAR/Note 81-7 (1981).

Figure Captions

Fig. 1 Arrangement of magnets for TARN including sextupole correction system.

Fig. 2 Line currents which induce the sextupole field.

Fig. 3 Illustration of the sextupole magnet with 6-fold symmetry. It is known the magnetic scalar potential ϕ_m only changes sign with the same absolute value for the rotation of $\pm\ \pi/3$ around s axis.

Fig. 4 (a) A mesh used for the field calculation of the sextupole magnet with the computer code TRIM.
(b) A plot of flux lines obtained by the computer code TRIM for the sextupole magnet.

Fig. 5 Calculated field structure of the sextupole magnet.

Fig. 6 Beam profiles in horizontal direction at TARN. Numbers in the figure show the RF-stacking numbers.

Fig. 7 Illustration of construction design of the sextupole magnet.

Fig. 8 Dimensions of three test pole shapes of the sextupole magnet.

Fig. 9 Measured field structures for three test pole shapes.

Fig. 10 Field mapping system with a temperature-controlled Hall-probe applied to the sextupole magnet.

Fig. 11 Mapped field strengths displayed on a graphic display by real time.

Fig. 12 Radial distribution of the integrated field strength of the sextupole magnet.

Fig. 13 (a) Integrated sextupole strength, $\int B''ds$, at the magnet axis obtained by the fitting to the data of $\int Byds$.
(b) The sextupole strength at the position of $s = 0$, $B''(0)$.
(c) The effective length of the sextupole magnet.

Fig. 14 Excitation characteristic of the sextupole magnet studied by a Hall-probe fixed at the position of $x = 100$ mm.

Fig. 15 Field measurement system by translation coils applied to the sextupole magnet.

Fig. 16 Illustration of the hard-wire connection between twin translation coils both in "Up" and "Down" states.

Fig. 17 Measured field structures for three excitation currents, 200 A, 300 A and 400 A.

Fig. 18 Measured field structures in three hofizontal planes, median plane and planes 15 mm apart up and down from the median plane.

Fig. 19 Field structure measured by a Hall-probe and twin translation coils.

Fig. 20 Excitation characteristic of the integrated sextupole strength measured by a Hall-probe and translation coils.

Fig. 21 Deviation of integrated sextupole strength.

Fig. 22 Dimensions measured at the time of alignment of sextupole magnets.

Fig. 23 Typical examples of working lines with sextupole system off (A) and on (B).

Fig. 24 ν - values for various RF seep frequencies. Solid and dashed lines represent cases where the sextupole system off and on, respectively.

Table Captions

Table 1 Specifications of the sextupole magnet for TARN.

Table 2 Dimensionless coefficients of polynomial expansion of integrated sextupole strength.

Table 3 Features of coefficients among magnets.

Table 4 Integrated sextupole strengths and their deviations from the average of all the twelve magnets.

Table 5 Precision of alignment of sextupole magnets.

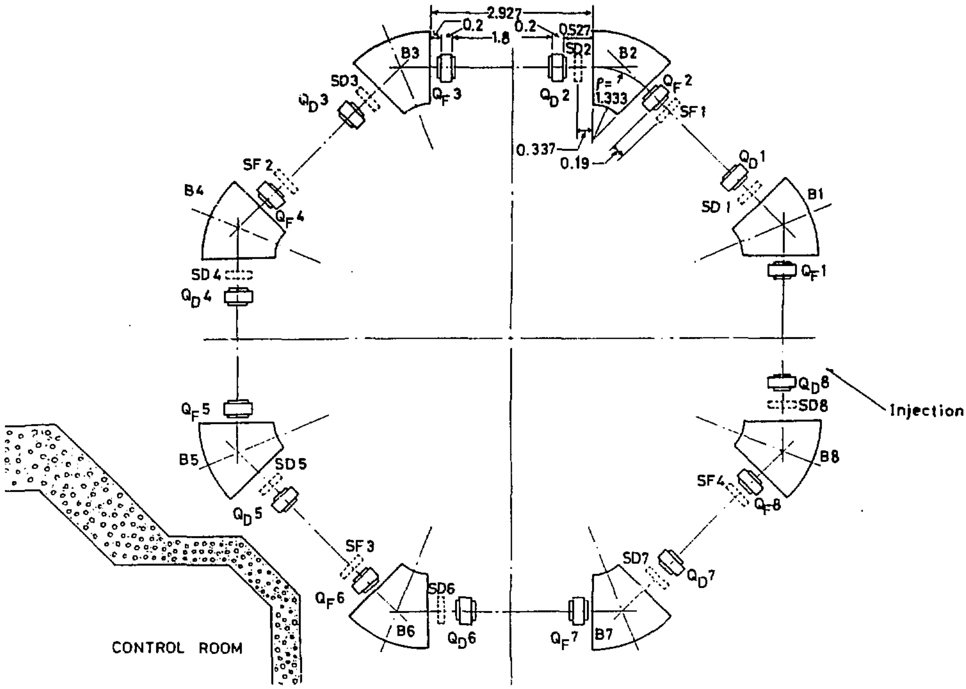

Fig. 1

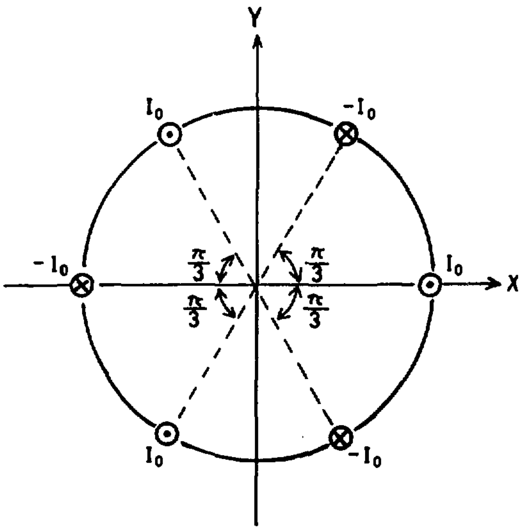

Fig. 2

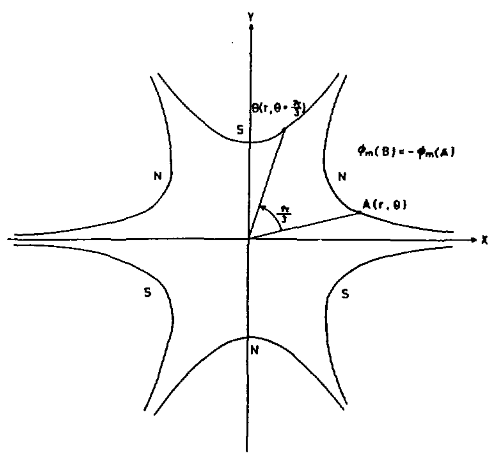

Fig. 3

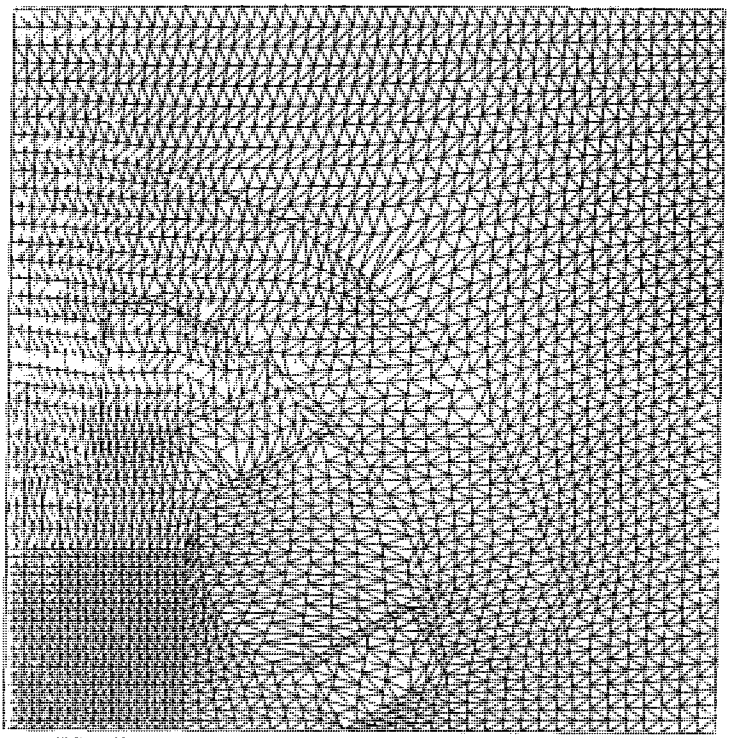

Fig. 4 (a)

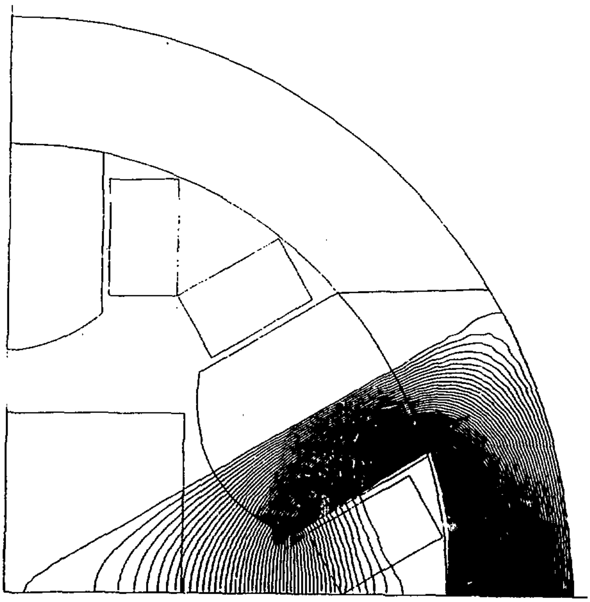

Fig. 4 (b)

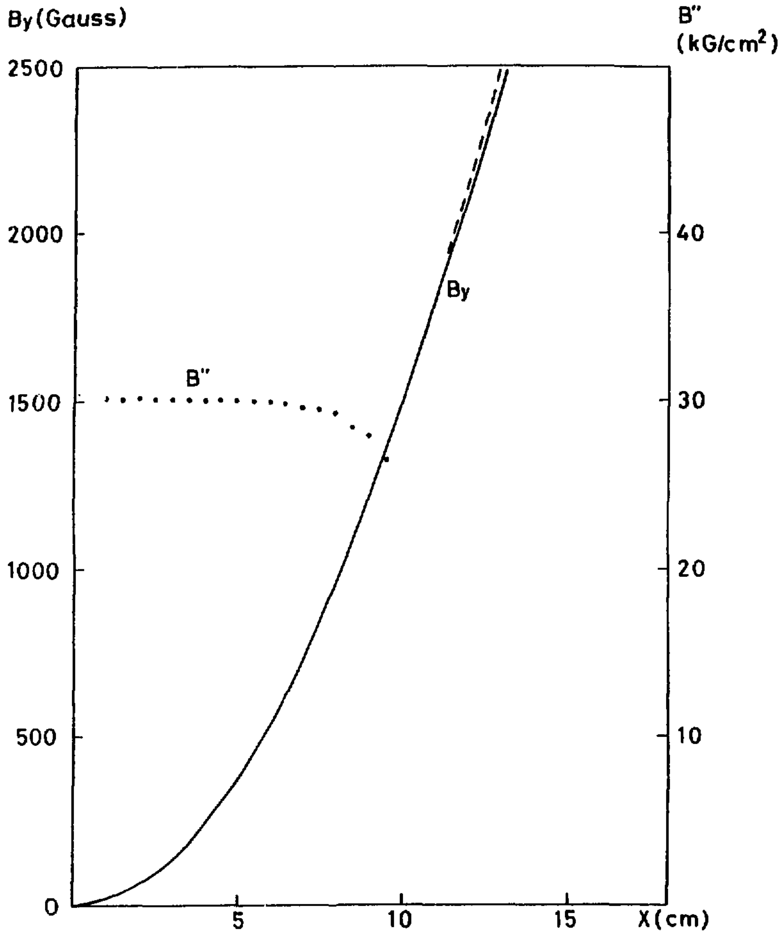
By(Gauss)
B''
(kG/cm^2)
2500
2000
1500
1000
500
0
40
30
20
10
By
B''
5
10
15
X(cm)

Fig. 5

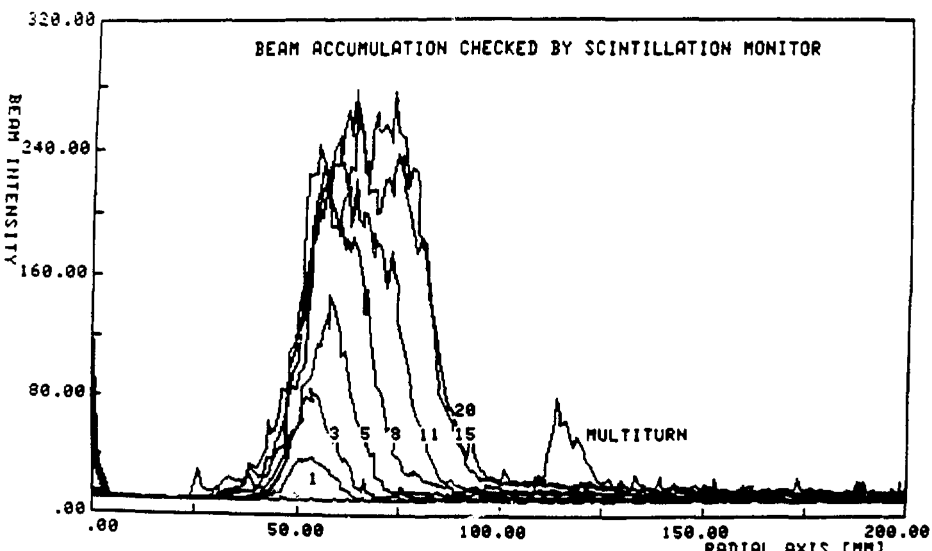
BEAM ACCUMULATION CHECKED BY SCINTILLATION MONITOR
BEAM INTENSITY
320.00
240.00
160.00
80.00
.00
.00
50.00
100.00
150.00
200.00
RADIAL AXIS [MM]
1
3
5
8
11
15
20
MULTITURN

Fig. 6

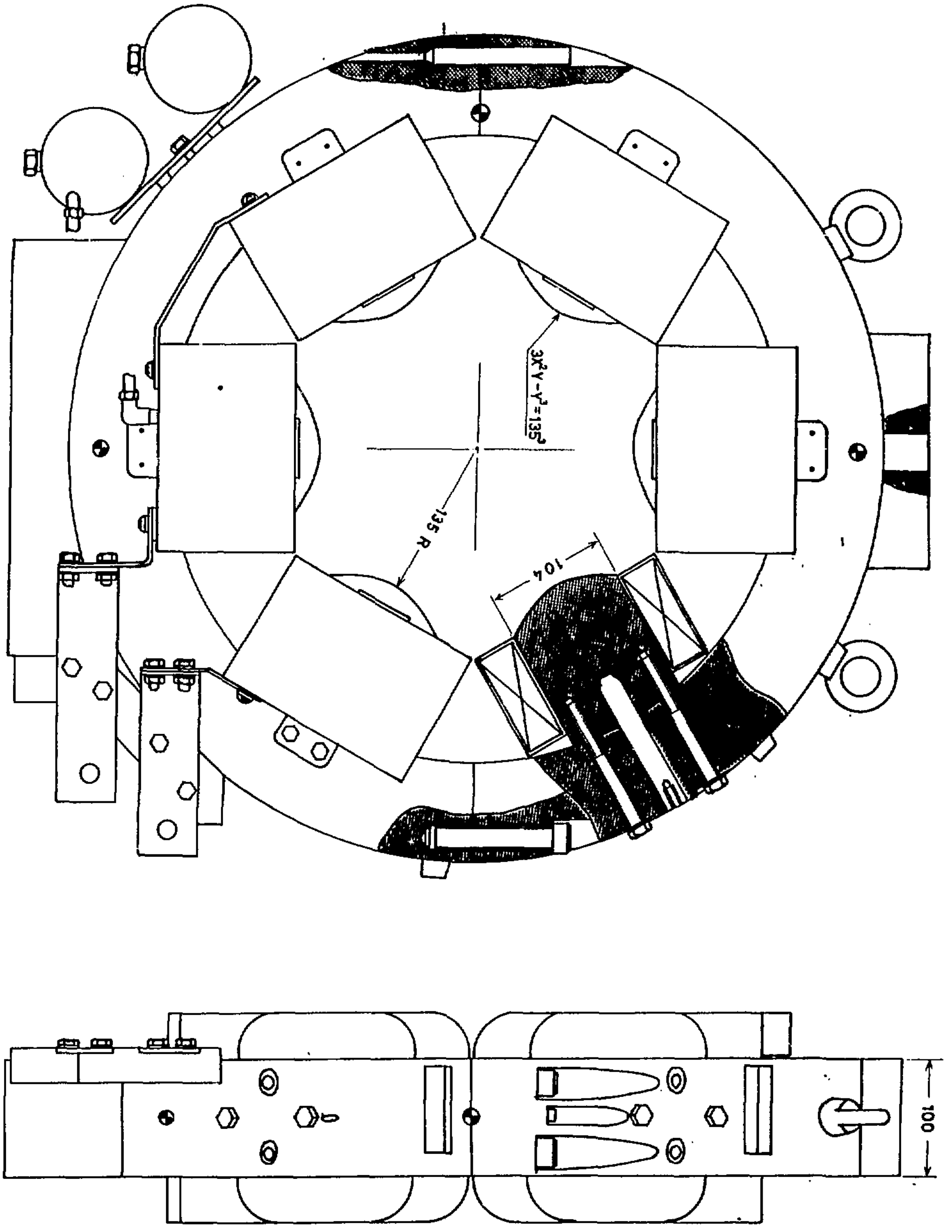

Fig. 7

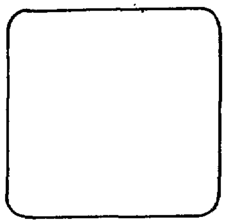

MODEL POLE

	A	B
1	0	0
2	30	47.5
3	30	55

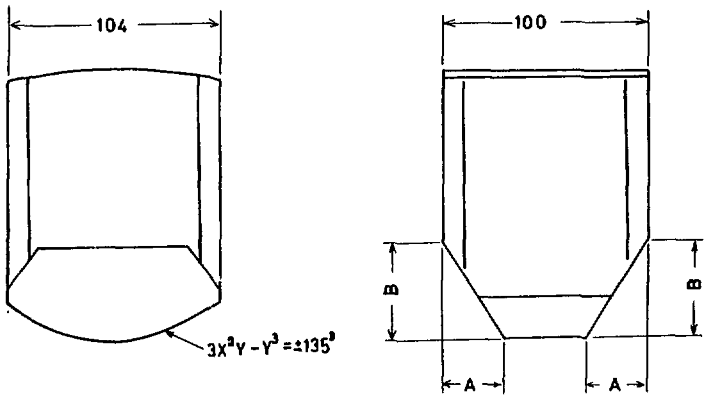

Fig. 8

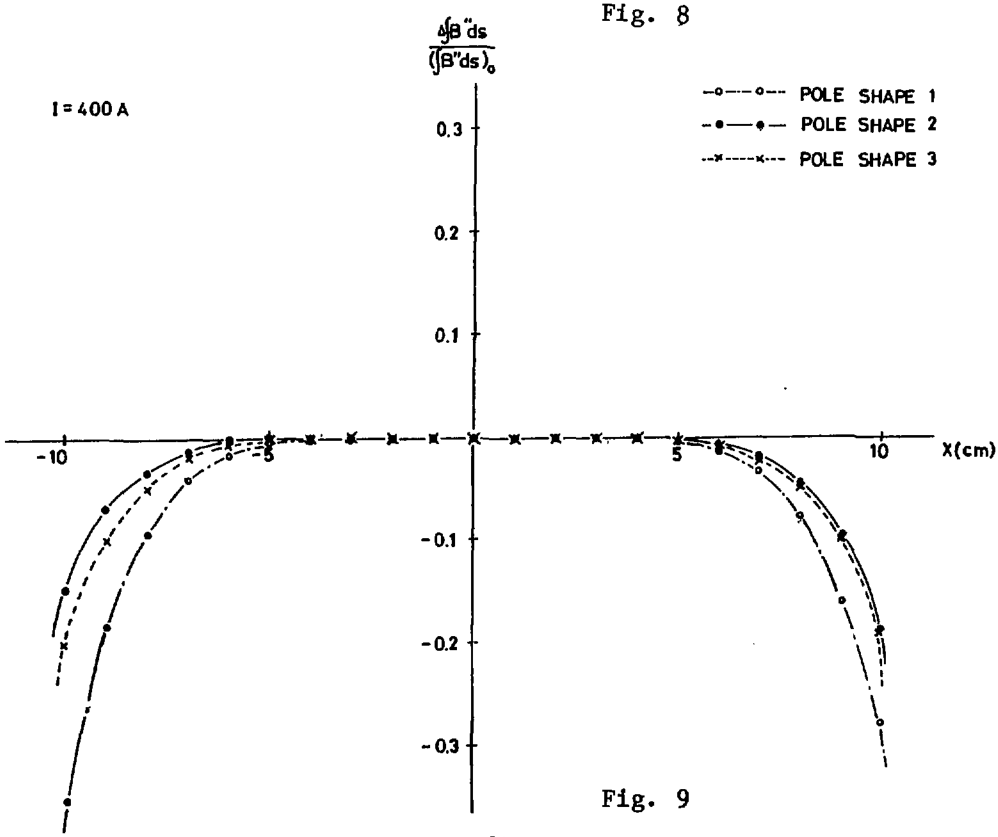

Fig. 9

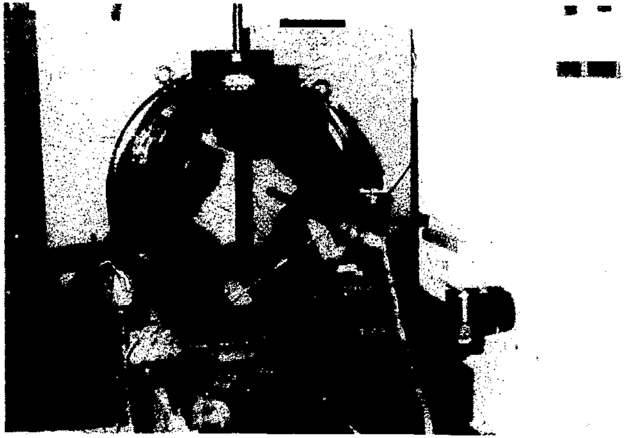

Fig. 10

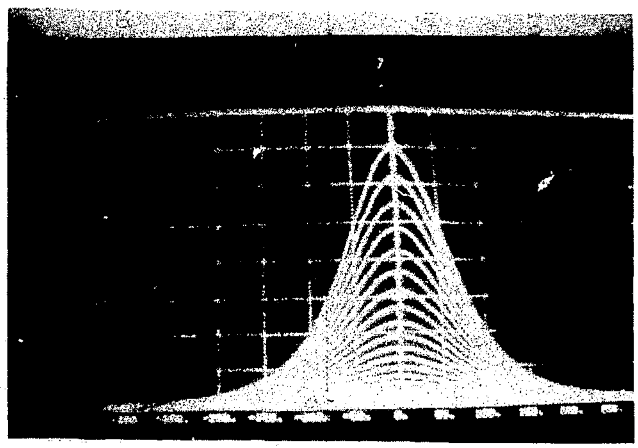

Fig. 11

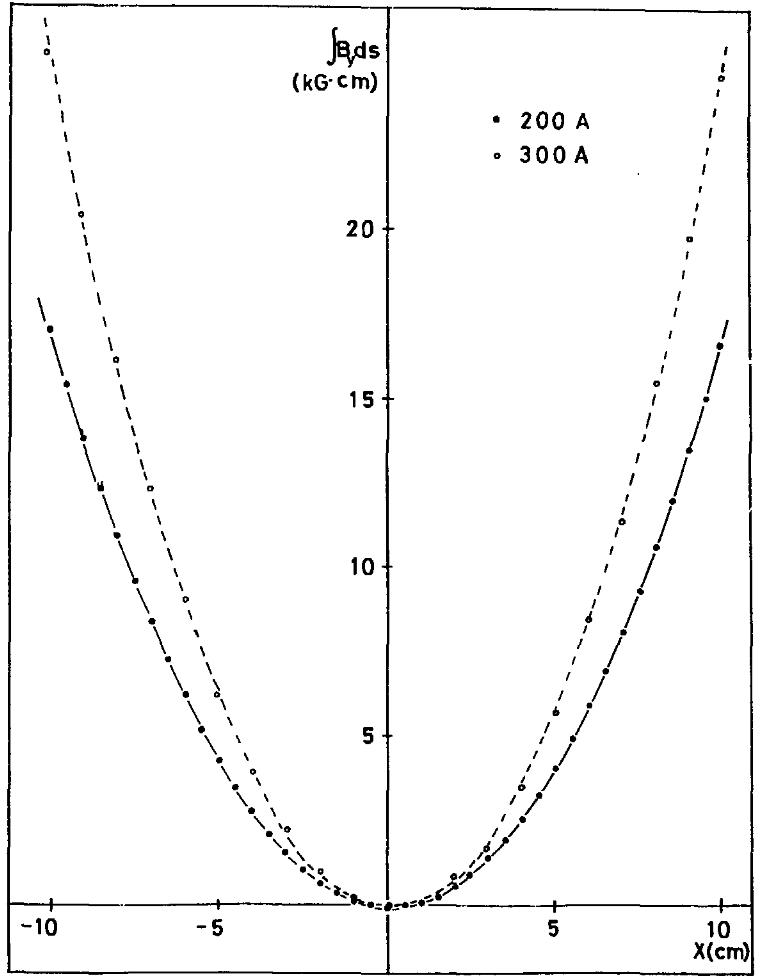

Fig. 12

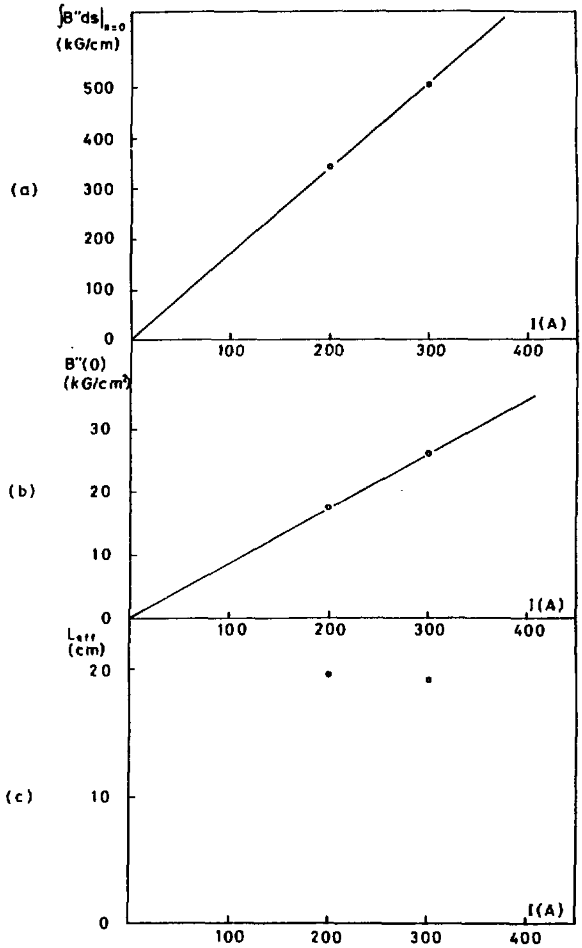

∫B''ds|s=0
(kG/cm)
500
400
(a)
300
200
100
0
I(A)
100
200
300
400
B''(0)
(kG/cm²)
30
(b)
20
10
0
I(A)
100
200
300
400
Leff
(cm)
20
(c)
10
0
I(A)
100
200
300
400

Fig. 13

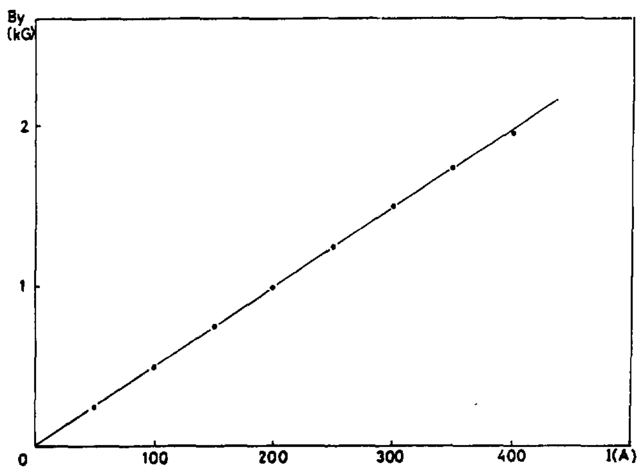

By
(kG)
2
1
0
100
200
300
400
I(A)

Fig. 14

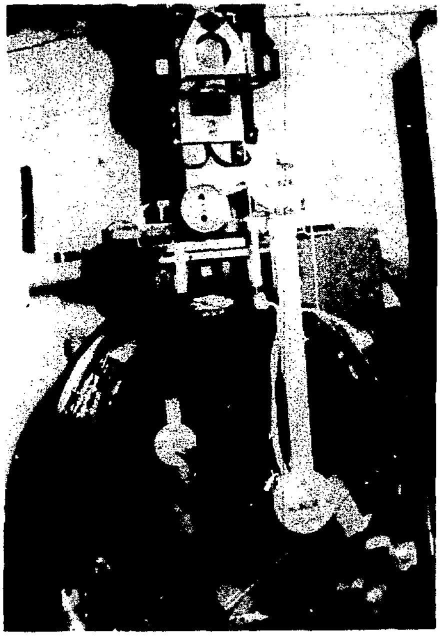

Fig. 15

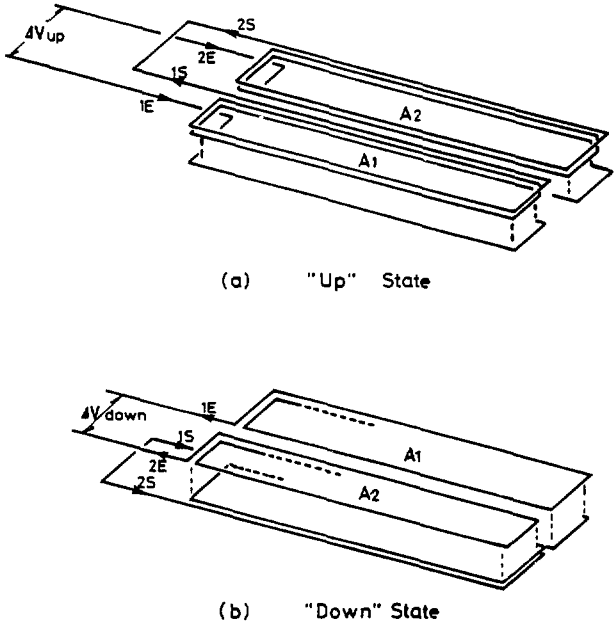

Fig. 16

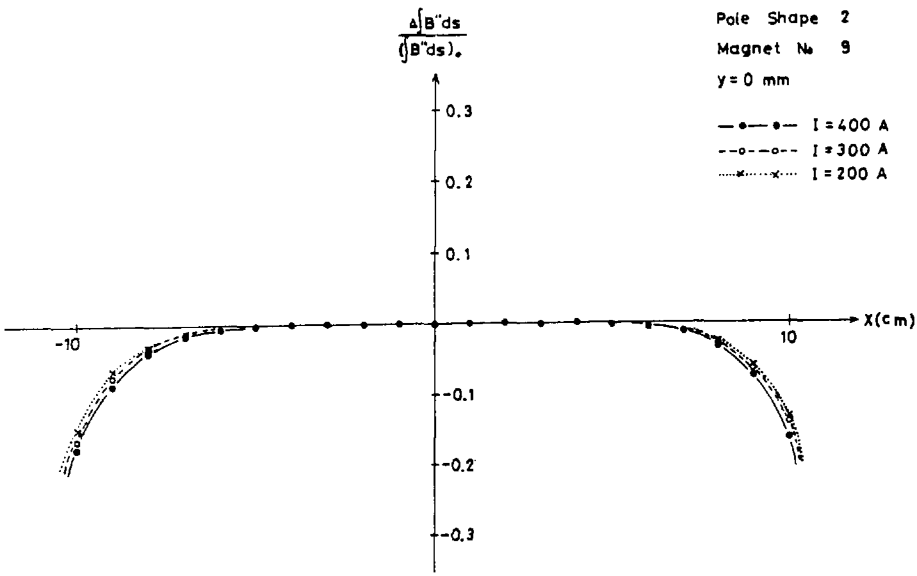

Fig. 17

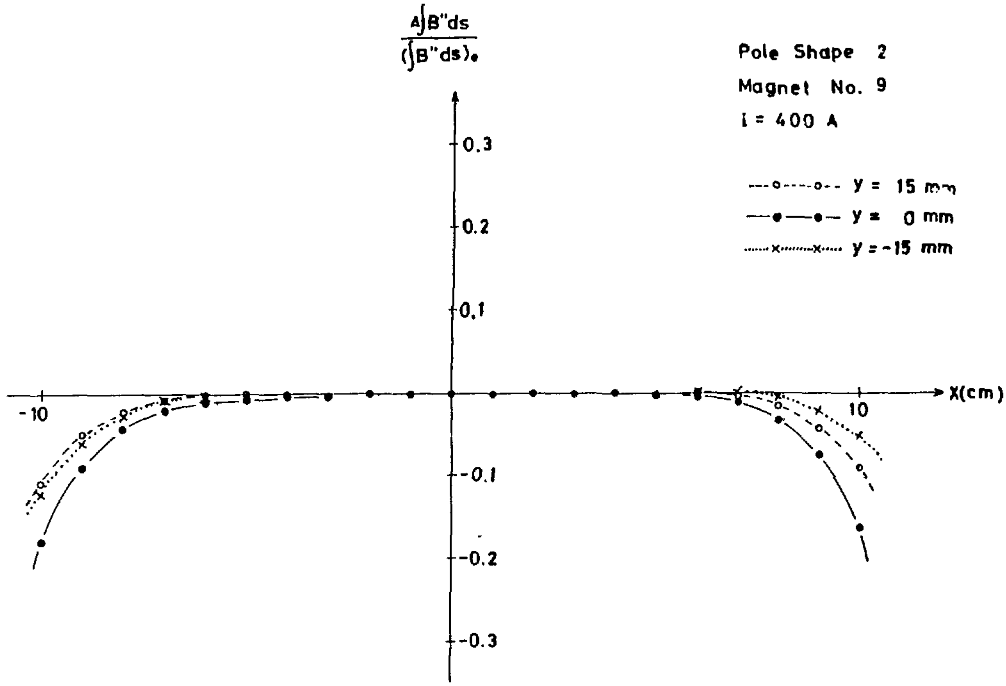

A∫B″ds / (∫B″ds)₀
Pole Shape 2
Magnet No. 9
I = 400 A
y = 15 mm
y = 0 mm
y = -15 mm
0.3
0.2
0.1
-0.1
-0.2
-0.3
-10
10
X(cm)

Fig. 18

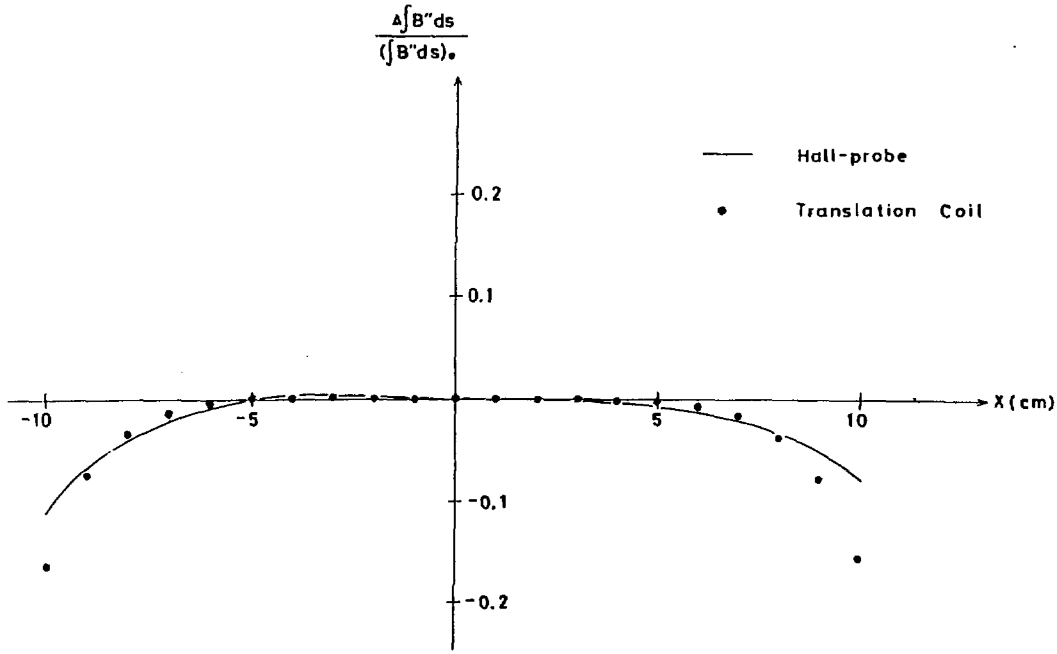

A∫B″ds / (∫B″ds)₀
Hall-probe
Translation Coil
0.2
0.1
-0.1
-0.2
-10
-5
5
10
X (cm)

Fig. 19

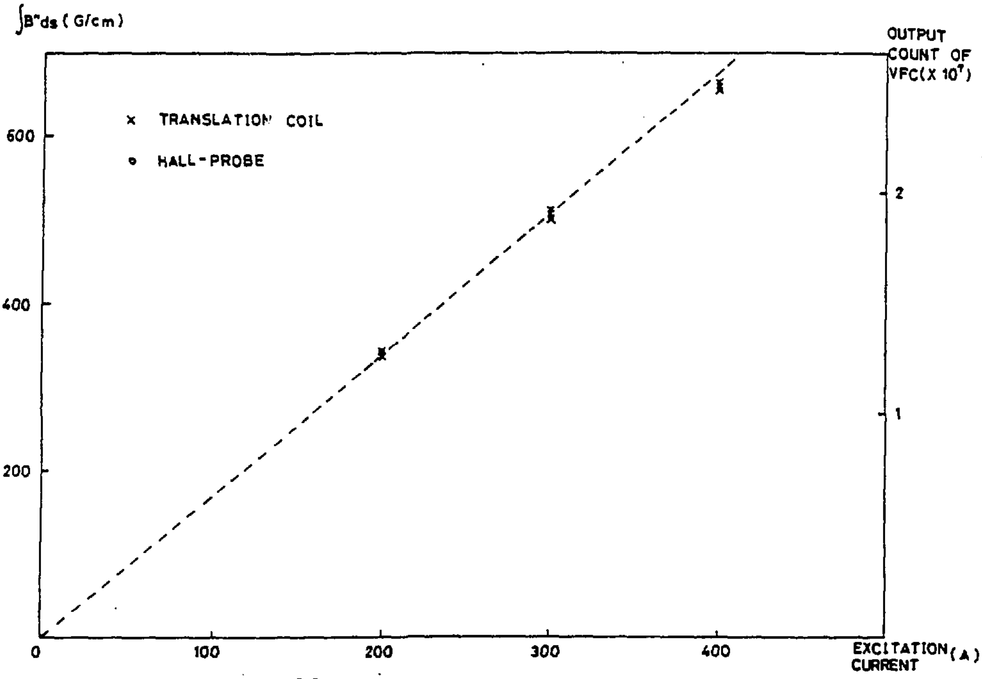

Fig. 20

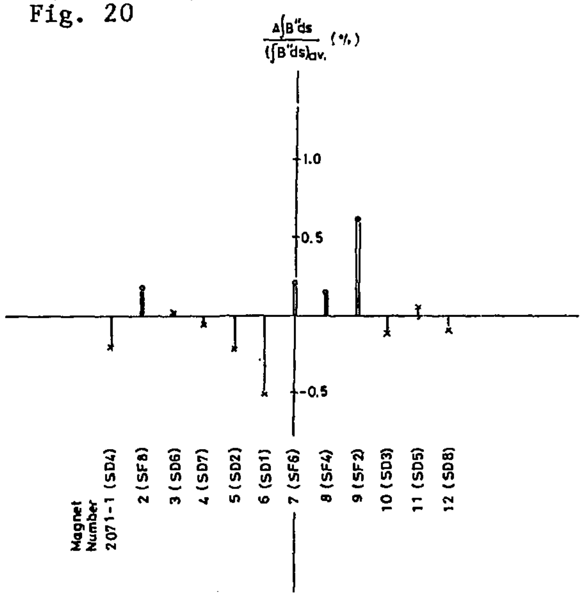

Fig. 21

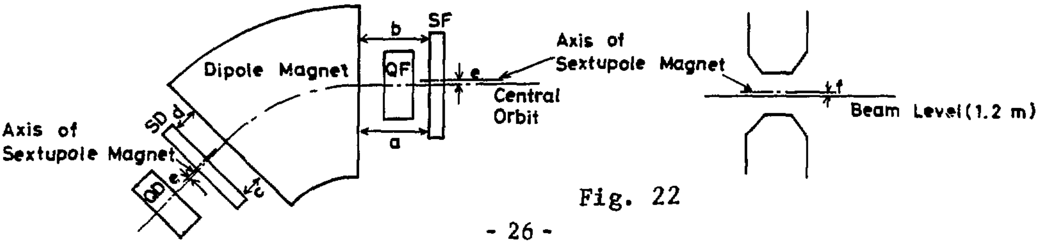

Fig. 22

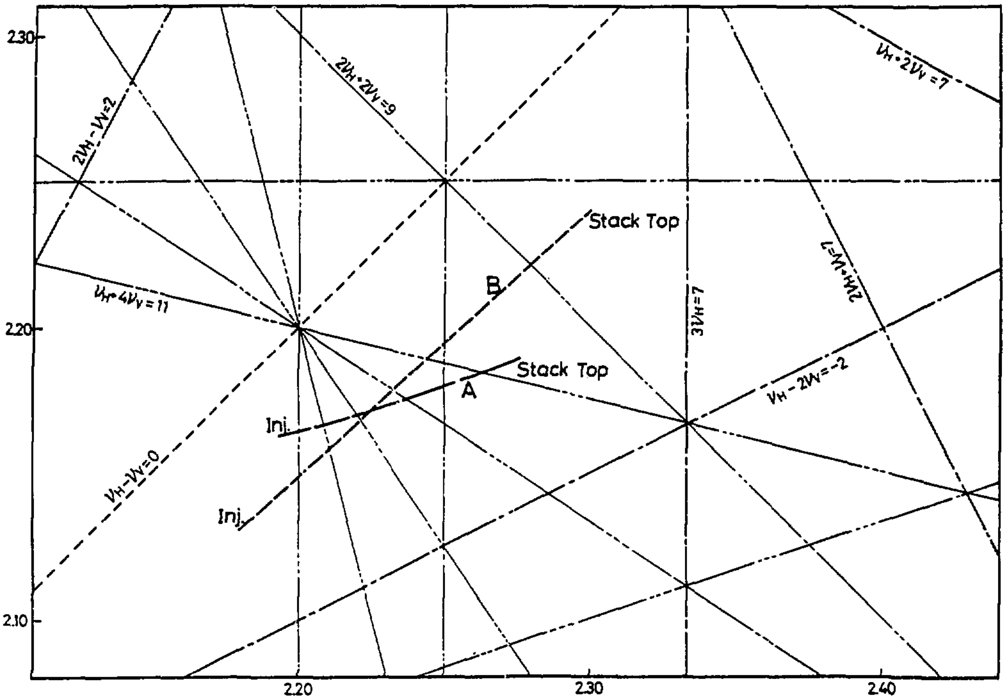

2.30
2.20
2.10
2.20
2.30
2.40
Stack Top
Stack Top
B
A
Inj.
Inj.
3νH=7
νH-2νV=-2
νH-νV=0

Fig. 23

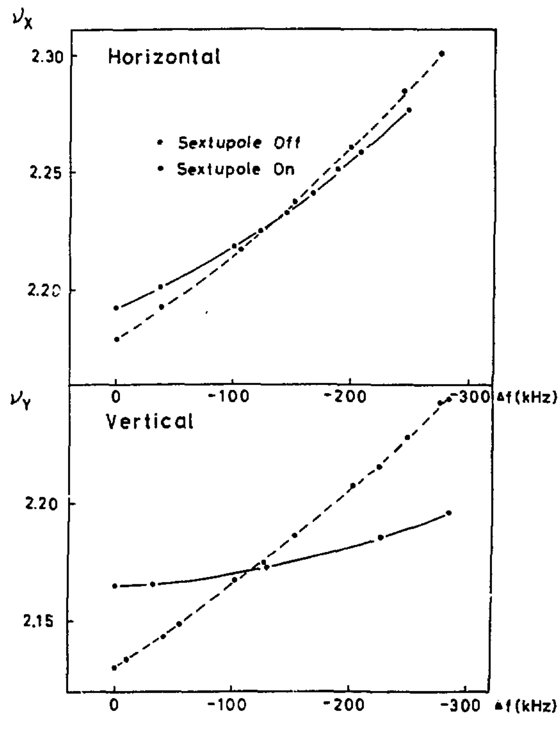

νX
Horizontal
Sextupole Off
Sextupole On
2.30
2.25
2.20
0
-100
-200
-300
Δf(kHz)
νY
Vertical
2.20
2.15
0
-100
-200
-300
Δf(kHz)

Fig. 24

Specifications of the Sextupole Magnet for TARN

Radius of the Inscribed Circle	135 mm
Pole Width	104 mm
Pole Shape	$3x^2y-y^3 = \pm 135^3$
Core Length	100 mm
Maximum B"	35 G/cm^2
Maximum Current	400 A
Maximum Current Density	13.33 A/mm^2
Number of Turns per Pole	41 Turns
Maximum Ampere Turns per Pole	16400 AT
Resistance of the Total Coil	89 mΩ (at 80 °C)
Maximum Power Dissipation	14.4 kW
Space Factor	0.506
Pressure Drop of Cooling Water	3 kg/cm^2
Flowing Rate of Cooling Water	3.5 ℓ/min
Total Weight of the Magnet	180 kg

Table 1

Magnet Number	Exitation Current (A)	z (mm)	a_1	a_2 $\times 10^{-3}$	a_3 $\times 10^{-2}$	a_4 $\times 10^{-2}$	a_5 $\times 10^{-1}$	a_6 $\times 10^{-1}$	a_7
			Coefficients of Polinomials						
1	400	0	0.9994	-3.316	-1.874	-3.287	1.379	1.194	-1.191
2	400	0	0.9992	6.749	-0.352	-5.501	1.232	2.080	-1.172
3	400	0	1.0005	6.152	-1.854	-5.530	1.022	1.048	-0.890
4	400	0	1.0004	-0.817	0.498	0.360	0.001	-0.205	-0.730
5	400	0	0.9995	5.319	-1.713	-4.177	2.126	1.286	-1.279
6	400	0	1.0007	-5.454	1.450	2.616	-0.643	0.511	-0.652
7	400	0	0.9999	2.070	-2.277	-1.351	2.339	0.936	-1.136
8	400	0	0.9998	6.606	-1.757	-1.733	1.776	1.032	-1.121
9	400	0	0.9998	6.971	-3.229	-4.515	2.436	1.223	-1.261
10	400	0	1.0008	2.177	-1.315	-0.131	1.334	0.033	-1.055
11	400	0	0.9998	-5.167	1.072	1.331	0.119	0.720	-1.014
12	400	0	0.9998	-0.665	-2.269	2.982	2.116	0.185	-1.237
6	300	0	1.0005	-3.359	3.975	-0.768	-1.572	1.236	-0.508
6	200	0	1.0010	1.891	5.136	-3.267	-2.139	1.798	-0.438
9	300	0	0.9997	2.234	-5.147	-2.554	0.618	0.896	-0.835
9	200	0	0.9994	6.986	1.108	-5.868	0.714	1.430	-0.557
6	400	-15	1.0015	5.006	-0.494	-5.395	1.808	1.604	-0.743
6	300	-15	0.9993	-8.146	-2.280	3.761	1.745	0.307	-0.564
6	200	-15	0.9989	5.530	5.207	-0.686	-0.658	0.663	-0.361
6	400	15	0.9987	6.522	0.845	-7.152	-0.507	1.821	-0.298
6	300	15	0.9996	1.283	4.859	0.147	-1.640	0.343	-0.179
6	200	15	0.9989	1.793	2.040	-3.294	-0.514	1.199	-0.289
9	400	-15	1.0002	-0.477	0.410	-3.872	1.573	2.559	-0.863
9	400	15	0.9999	-1.275	0.759	1.968	0.531	-0.184	-0.657

Table 2

Table 3

Coefficients	Obtained Results among Magnets
a_1	0.9992 ∿ 1.0008
a_2	- 0.005 ∿ + 0.007
a_3	- 0.03 ∿ + 0.02
a_4	- 0.06 ∿ + 0.03
a_5	- 0.06 ∿ + 0.24
a_6	- 0.02 ∿ + 0.21
a_7	- 0.65 ∿ - 1.28

Table 4

Magnet No.	$\int B''ds$ kG/m	$\frac{\Delta(\int B''ds)}{(\int B''ds)_{AV}}$ (%)
2071-1	65.62	- 0.21
2	65.87	0.17
3	65.77	0.02
4	65.72	- 0.05
5	65.61	- 0.22
6	65.42	- 0.51
7	65.89	0.20
8	65.85	0.14
9	66.16	0.62
10	65.68	- 0.12
11	65.79	0.05
12	65.69	- 0.10
Average	65.76	

Table 5 Precision of alignment of sextupole magnets.

Dimension	Ideal Value	Deviation from the Ideal Value
a	540.0 mm	- 0.15 ∿ - 0.04 mm
b	540.0	- 0.12 ∿ - 0.01
c	287.0	+ 0.08 ∿ + 0.22
d	287.0	+ 0.03 ∿ + 0.22
e	0.0	- 0.05 ∿ + 0.05
f	0.0	+ 0.00 ∿ + 0.03